Influence of Welding Temperature on Material Flow During Friction Stir Welding of AZ31 Magnesium Alloy

S. MIRONOV, Y.S. SATO, and H. KOKAWA

In this work, the effect of welding temperature on material flow during friction stir welding (FSW) of AZ31 magnesium alloy was examined. To this end, FSW was conducted in the temperature range of 0.65-0.85 T_m (T_m is the melting point) and sample-scale EBSD mapping was employed to characterize texture distribution. Despite that the low-temperature welds contained macro-scale defects (which presumably affected material flow), several important observations were made. In the entire temperature range, the global material motion was shown to consist of two principal components, viz. shoulder-induced flow and probe-induced flow. In some cases, however, a synergetic effect of these two constituents resulted in transitional orientation of macro-scale shear plane thus giving rise to a transitional material flow. During low-temperature FSW, the global material transportation was dominated by the probe. However, the contribution of the shoulder and transitional components was found to increase with welding temperature. This effect was attributed to the dominant role of the shoulder in generation of FSW heat. Above ~ 0.8 T_m, however, the transitional material flow was found to abruptly disappear. This result was associated with reduction of temperature sensitivity of flow stresses and the resulting equilibration of their distribution within the stir zone.

https://doi.org/10.1007/s11661-019-05194-0

I. INTRODUCTION

FRICTION stir welding (FSW) is a relatively new solid-state joining technique having significant industrial potential. Basically, FSW involves a plunging of a rapidly rotating welding tool between two butted sheets and its subsequent traverse along the joint line. Due to the frictional heating as well as plastic deformation induced by the rotating tool, the local temperature of the welded material raises so it can be deformed at relatively low stress. Accordingly, the hot material flows around the tool, fills the cavity at its rear, and thus forms a solid-state joint. The welding tool typically has a mushroom-type design and consists of a relatively large shoulder and a relatively small threaded probe. Further details of FSW are available in recent reviews on the subject.[1–3]

The feasibility of FSW for material joining and service properties of produced welds are believed to be essentially influenced by *material flow* during welding. Accordingly, this issue has attracted significant interest. An extensive research has conclusively demonstrated the remarkable complexity of this process. Its principal characteristics are briefly reviewed below.

Due to a specific character of FSW process, the stirred material normally experiences a combination of rotational and translation motions. In order to improve material mixing, however, the material may additionally be forced to flow along the height of the welding tool. This effect is usually achieved by the probe threading which promotes downward material transportation and the respective upward extrusion of excessive material.[1–3] As a result, the stirred material is thought to follow a very complex helical trajectory.

Moreover, considering the characteristic design of the welding tool, the material motion is well accepted to be essentially different in the upper portion and remaining parts of the stir zone. Specifically, the material flow in the near-surface layer is governed by the tool shoulder, whereas that in the bulk stir zone is driven by the tool probe.[4,5] In both cases, the imposed strain is close to simple-shear deformation,[6–10] but the shear occurs

S. MIRONOV is with the Belgorod National Research University, Pobeda 85, Belgorod, Russia, 308015. Contact e-mail: mironov@bsu.edu.ru Y.S. SATO is with the Department of Materials Processing, Graduate School of Engineering, Tohoku University, 6-6-02 Aramaki-aza-Aoba, Sendai 980-8579, Japan. H. KOKAWA is with the Department of Materials Processing, Graduate School of Engineering and also with the School of Materials Science and Engineering, Shanghai Jiao Tong University, 800 Dongchuan Road, Minhang District, Shanghai 200240, P.R. China.

Manuscript submitted November 4, 2018.
Article published online March 22, 2019

either along the shoulder plane or the probe surface. In the transition zone, interaction between these two motions may result in chaotic material flow.[1] Under some circumstances, however, such interaction may also give rise to a macro-scale effect at which the shear plane lies between the shoulder surface and the probe surface (the so-called ''truncated cone'' model).[11]

In some cases, FSW is considered as an *in situ* extrusion process wherein the tool, the weld backing plate, and cold base material outside the weld zone form an ''extrusion chamber'' which moves relative to the welded workpieces.[12,13] The set of material layers extruded during each tool revolution creates a characteristic ''onion ring'' structure in the stir zone.[14] It is interesting to note that the material may experience several rotations around the tool before its final deposition in the stir zone.[15,16]

The combination of the rotation and translation motions of the tool gives rise to a characteristic asymmetry of FSW: the advancing side (AS), where the direction of the tool rotation is the same as that of the tool translation, and the retreating side (RS), where they are opposite. The material flow on the AS is believed to be relatively stagnant and may result in a wormhole defect,[15,17–20] but the nature of this undesirable effect is not completely clear. Tool advance per rotation (or *weld pitch*) is considered to be an important characteristic of FSW which may essentially influence the material flow. Specifically, its increment is believed to suppress the vertical material transportation[2] and promotes welding defects.[21,22]

Due to the thermo-mechanical character of FSW, the induced material flow should be a function of temperature. However, the current understanding of the temperature effect is still limited, to the best of the authors' knowledge. The present work attempted to fill this gap in our knowledge. To this end, FSW was conducted in wide interval of welding temperatures and the induced material flow was studied through the analysis of texture distribution within the stir zone.

II. EXPERIMENTAL PROCEDURES

The program material employed in the present investigation comprised a commercial AZ31 magnesium alloy with nominal chemical composition of Mg-3.0Al-1.0Zn (wt.pct) supplied by Osaka Fuji Kogyo (Japan). Plastic deformation of magnesium is well accepted to be dominated by a sole basal slip and, therefore, interpretation of this process is relatively easy. The base material condition was produced by extrusion at 350 °C and subsequent annealing for 2 hours at 300 °C which resulted in a relatively coarse-grained (~ 200 μm) microstructure and a moderately strong $\{hkil\}<1\bar{2}10>$ fiber texture. The material was supplied as 4-mm-thick sheets. Further details on the initial microstructure have been reported elsewhere.[23]

The received material was friction stir welded in a bead-on-plate configuration. In order to investigate material flow at different welding temperatures, FSW was conducted in a relatively wide interval of tool rotational rates, from 300 to 3000 rpm. On the other hand, the tool travel speed was kept constant at 200 mm/min in all cases. The nomenclature of the material conditions studied is summarized in Table I. The welding tool was manufactured from a tool steel and consisted of a concave shoulder with a diameter of 15 mm and an M5 threaded cylindrical probe with a rounded tip. Further details of the tool geometry are given in Figure 1. FSW was performed under plunge-depth control and the tool tilting angle was 3 deg in all cases. The typical conventions of FSW geometry were adopted in this study, i.e., the welding, transverse, and normal directions were denoted as WD, TD, and ND, respectively.

The welding temperature was measured by K-type thermocouples placed directly on the weld seam (Figure 2(a)). The peak recorded temperature was defined as the welding temperature. The temperature was found to increase with the tool rotational rate from ~ 0.57 T_m at 300 rpm to ~ 0.85 T_m at 2000 rpm (where T_m is the melting point) and then tended to saturate at this level (Figure 2(b)).

For examination of the material flow, the produced welds were sectioned orthogonal to the welding direction. For preliminary optical observations, the microstructural samples were prepared using conventional metallographic techniques followed by final etching in a solution of 4.2 g picric acid + 66 mL ethanol + 10 mL acetic acid + 10 mL distilled water. To examine the influence of the welding temperature on stir zone size, its cross-sectional area was measured using Winroof image-processing software. To investigate texture distribution within the stir zone, electron backscatter diffraction (EBSD) was applied. The surface finish for EBSD was produced by electro-polishing in a commercial AC2 Struers polishing solution at near-zero temperature (ice bath) and an applied potential of 40 V. EBSD analysis was conducted using Hitachi S-4300SE and JEOL JSM-7800F field emission gun scanning electron microscopes equipped with the TSL OIM^{TM} EBSD system and operated at an accelerated voltage of 25 kV. Depending on particular purpose, different scan step sizes were used for mapping. Specifically, low-resolution (sample-scale) EBSD maps were acquired using a scan step size of 5 μm. On the other hand, considering a variation of mean grain size in

Table I. Nomenclature of Studied Material Conditions

Tool Rotational Speed, rpm	Weld Pitch, mm	Welding Temperature, T_m
300	0.6667	0.57
400	0.5000	0.64
500	0.4000	0.65
600	0.3333	0.67
700	0.2857	0.72
800	0.2500	0.71
900	0.2222	0.76
1000	0.2000	0.75
1500	0.1333	0.79
2000	0.1000	0.84
2500	0.0800	0.85
3000	0.0667	0.85

different welds from 2 to 40 μm,[23] high-resolution EBSD maps were obtained using step sizes ranging from 0.2 to 0.5 μm. The average confidence index for each EBSD map ranged from 0.13 to 0.61. By comparison, experiments on face-centered cubic metals have shown that the fraction of correctly indexed patterns with confidence index greater than 0.1 is 95 pct.[24]

III. RESULTS

A. *Optical Observations*

The typical low-magnification optical images of welds produced at different welding temperatures are summarized in Figure 3. For clarity, a tool profile is also shown as dotted line.

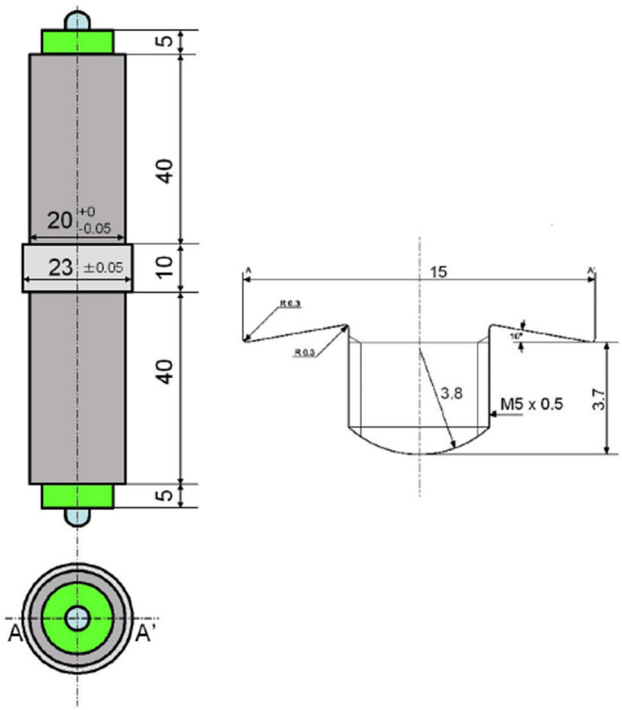

Fig. 1—Schematic of welding tool.

In the weld produced at the lowest temperature, the stir zone resembled closely the shape of the tool probe (Figure 3(a)). This presumably indicated the dominant role of the probe in material flow during FSW. Moreover, a tunnel-type defect was also found at the weld root (Figure 3(a)). With an increase in the welding temperature, the upper section of the stir zone became enlarged (solid arrows in Figure 3(b)), thereby reflecting an increase of the shoulder influence on the material transportation. On the other hand, the welding defect tended to disappear (Figure 3(b)). At the highest temperature of ~ $0.85T_m$, the upper section of the stir zone became very pronounced (Figures 3(c) and (d)), presumably evidencing a considerable contribution of the tool shoulder to the material motion. Another important observation was that the remaining section of the stir zone acquired an elliptical shape (Figures 3(c) and (d)), thus indicating a possible change in the character of the material flow.

Attempting to quantify the observed effects, the cross-sectional area of the stir zone (excluding welding defects) was measured as a function of the welding temperature, as shown in Figure 4(a). It is clear that the stir zone size increased with temperature. This observation was quite expectable and most likely originated from the well-known material softening at high temperatures. To provide further insight into this phenomenon, the intercept width of the stir zone was measured in its upper and mid-thickness sections, as shown in Figure 4(b); in the former case, the width was measured approximately 250 μm below the weld surface. It is clear from the figure that the tool shoulder primarily contributed to the enlargement of the stir zone size in the entire temperature range studied. At the highest welding temperatures, however, the material volume swept by the tool probe also increased, thus mirroring the change of the stir zone shape (arrows in Figures 3(c) and (d)).

From the preliminary observations, therefore, it seems that the contribution of the tool shoulder into global material transportation enlarged with temperature.

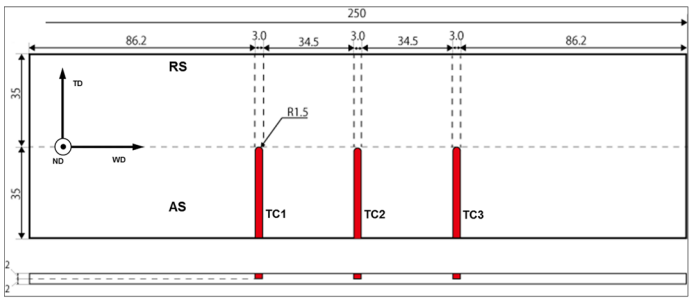

(a)

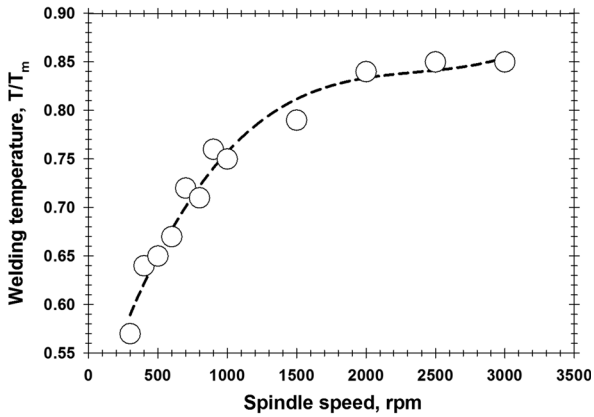

(b)

Fig. 2—(*a*) Layout of thermocouples inside workpiece (unit: mm) and (*b*) effect of spindle speed on welding temperature. In (a), TC1, TC2, and TC3 are thermocouples of numbers 1, 2, and 3, respectively; RS and AS are retreating side and advancing side, respectively.

B. *EBSD Measurements*

To provide deeper insight into the material flow, sample-scale EBSD maps were taken from the produced welds, typical examples being summarized in Figure 5.*

*Here and hereafter, a reader is referred to on-line version of this paper to see figures in color.

It is evident from the figure that the stir zones were characterized by fairly inhomogeneous texture distribution and this effect was most pronounced in low-temperature welds (Figures 5(a) and (b)). The particularly heterogeneous (or even irregular) character of texture in these cases was essentially associated with welding defects (black domains in Figures 5(a) and (b)) which presumably disturbed the normal character of material flow. In such cases, the obtained results were probably not sufficient to completely ascertain the regular material motion occurring during low-temperature FSW. Nevertheless, several important suggestions may be drawn from the available EBSD data and these are considered below.

In accordance with the works by Suhuddin *et al.*[4] and Mironov *et al.*,[23] the texture substantially varied throughout the thickness of all studied welds (Figure 5). To get more fundamental insight into this phenomenon, (0001) and $(11\bar{2}0)$ pole figures were extracted from characteristic microstructural regions. Data analysis showed that the texture distribution was somewhat different in the welds produced below and above ~ 0.75 T_m and typical examples are given in Figures 6 and 7, respectively**. The schematics of the texture distributions for these characteristic cases are shown in Figure 8.

**The textural data shown in these figures were derived from the regions numbered in Figures 5(b) and (c), respectively.

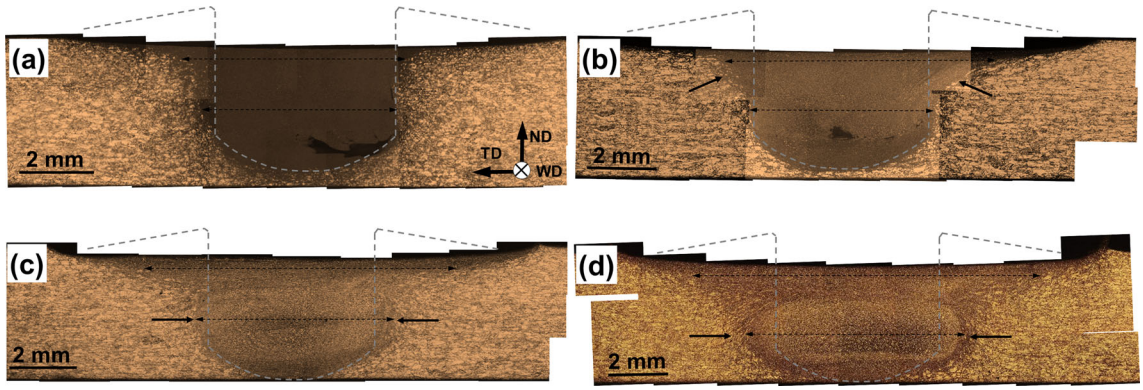

Fig. 3—Low-magnification optical images of transverse cross sections of the welds produced at the welding temperatures of (*a*) $0.57T_m$, (*b*) $0.75T_m$, (*c*) $0.84T_m$, and (*d*) $0.85T_m$. For clarity, tool profile (dotted line) is shown. Solid arrows indicate the increment of the stir zone area. Dotted arrows show approximate locations of measurements of stir zone width. In all cases, the retreating side is the left side and the advancing side is the right side. Note: During FSW, the gap between the tool shoulder and workpiece, which is apparent from the figure, was presumably filled by the material extruded from the tool keyhole.

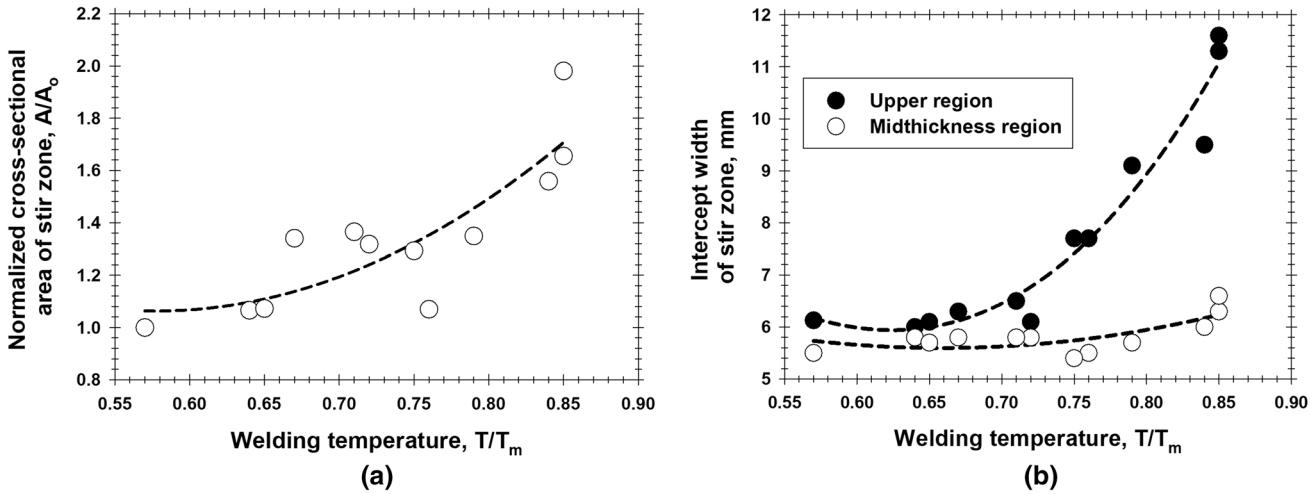

Fig. 4—Effect of welding temperature on (*a*) normalized cross-sectional area of stir zone and (*b*) intercept widths of stir zone. Note: A_0 is the cross-sectional area of the stir zone at the lowest welding temperature.

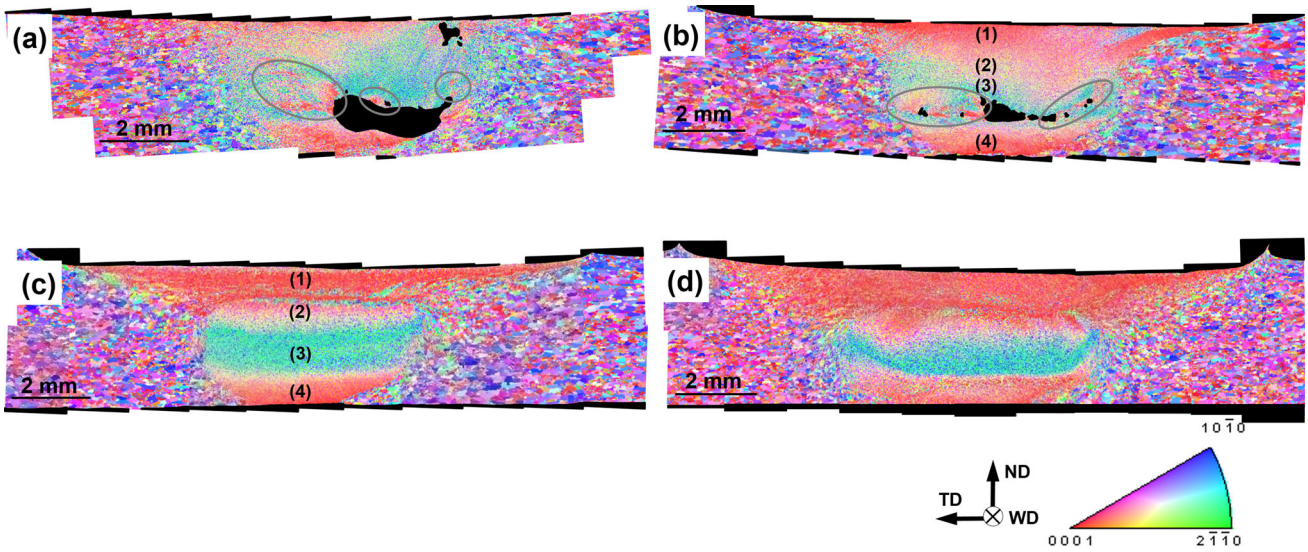

Fig. 5—Sample-scale EBSD maps showing grain orientations relative to the ND in the welds produced at the welding temperatures of (*a*) 0.65 T_m, (*b*) 0.75 T_m, (*c*) 0.84 T_m, and (*d*) 0.85 T_m. The color code triangle is shown in the bottom right corner. In all cases, the retreating side is the left side and the advancing side is the right side. The textural data derived from the regions indicated in (b) and (c) are shown in Figs. 6 and 7, respectively. See Section III–B for details (Color figure online).

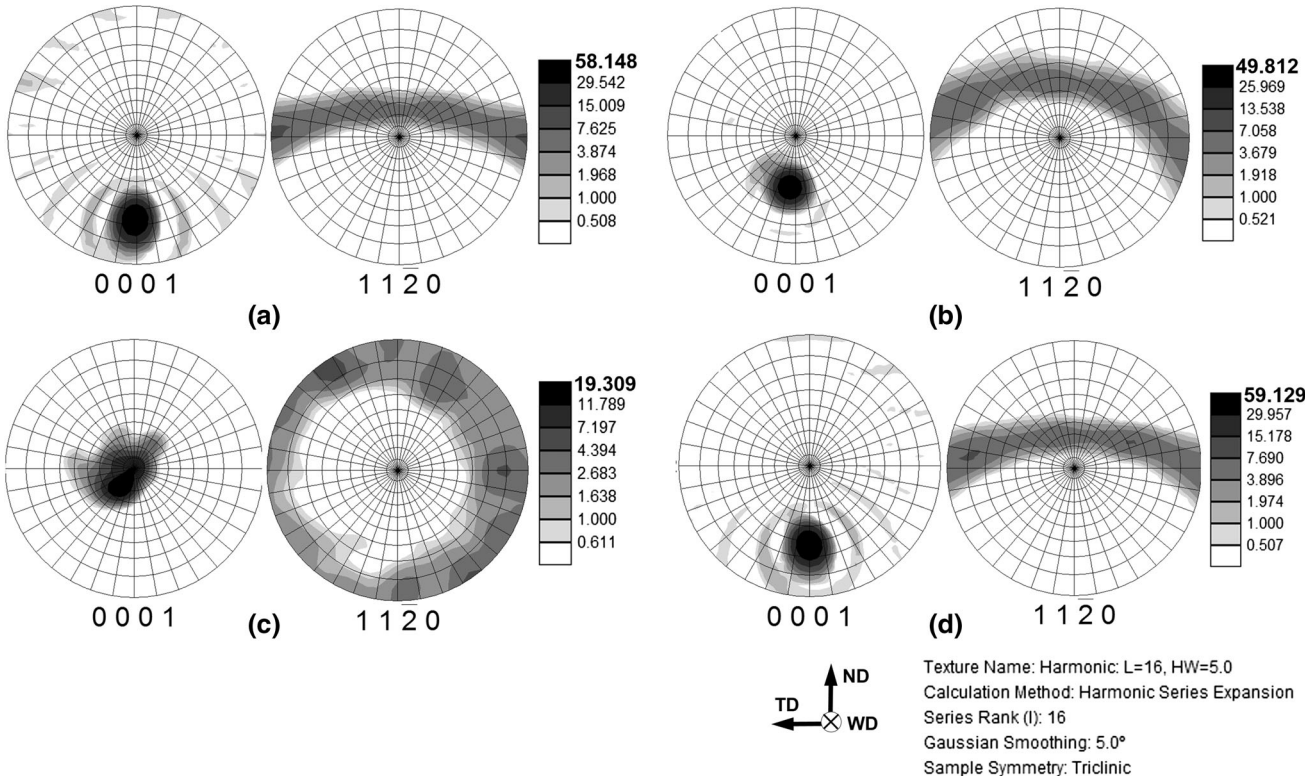

Fig. 6—Characteristic throughout-thickness texture distribution in a typical low-temperature weld: (*a*) upper region (area (1) in Fig. 5b), (*b*) transitional region (area (2) in Fig. 5b), (*c*) mid-thickness region (area (3) in Fig. 5b), and (*d*) bottom region (area (4) in Fig. 5b). See Section III–B for details.

In both cases, the textural patterns were characterized by a number of similarities. Specifically, the texture in the upper section of the stir zone was dominated by a nearly <0001>//ND orientation (Figures 6(a), 7(a) and 8), thus presumably evidencing the prevalence of shoulder-induced material flow. In contrast, the basal planes at the weld mid-thickness were aligned closely with the probe column surface (Figures 6(c), 7(c), and 8). According to Park *et al.*,[25] this observation may be interpreted in terms of material motion governed by the

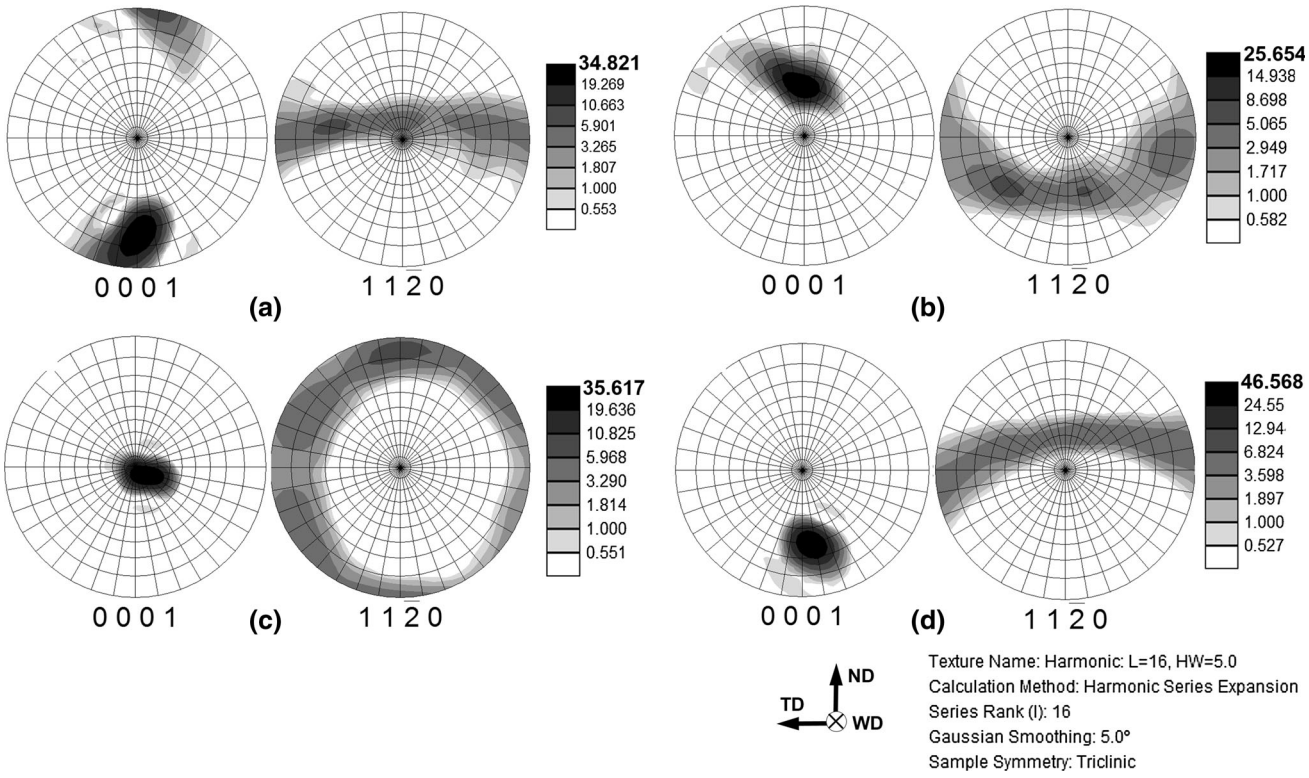

Fig. 7—Characteristic throughout-thickness texture distribution in a typical high-temperature weld: (*a*) upper region (area (1) in Fig. 5c), (*b*) transitional region (area (2) in Fig. 5c), (*c*) mid-thickness region (area (3) in Fig. 5c), and (*d*) bottom region (area (4) in Fig. 5c). See Section III–B for details.

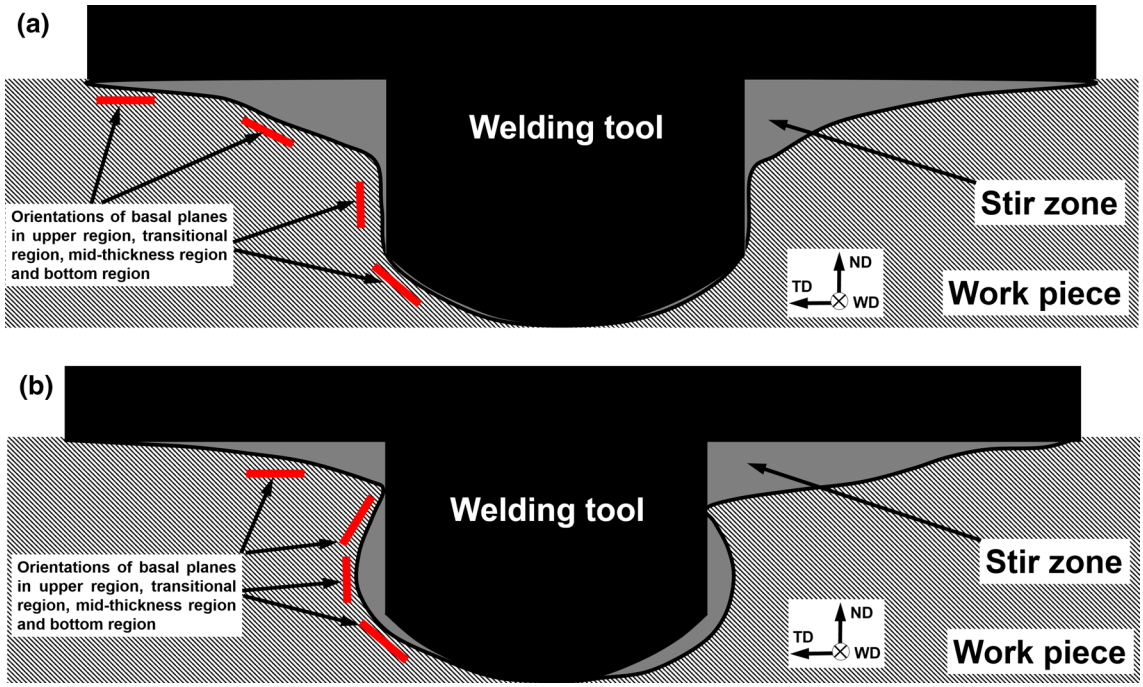

Fig. 8—Schematic of the distribution of orientation of basal planes throughout the thickness of (*a*) low-temperature welds and (*b*) high-temperature welds. See Section III–B for details.

tool probe. In the bottom region, the orientation of the basal planes enables to associate the material flow with the probe tip (Figures 6(d), 7(d) and 8), thereby also reflecting the probe-induced material flow.

On the other hand, material flow in the transition zone between the shoulder and the probe was distinctly different at low and high temperatures. In the former case, the basal planes were characterized by a transitional orientation between the shoulder and probe surfaces (Figures 6(b) and 8(a)). According to Reynolds *et al.*,[11] this phenomenon may be attributed to a synergetic effect of the shoulder and the probe on the material motion, and is known to as the "truncated cone" model. In contrast, the orientation of the basal planes in the high-temperature welds was distinctly different (compare Figures 6(b) and 7(b)). In such cases, the produced texture seems to be rather attributable to the elliptical shape of the stir zone observed at high temperatures (Figures 7(b) and 8(b)) and, if so, it probably originated from the probe-induced material flow. Assuming that the welding defects exerted no principal influence on mutual contributions of the shoulder-induced, probe-induced, as well as transient components of material flow, these were quantified from the sample-scale EBSD maps in Figure 5. To this end, the following procedure was adopted. In the upper half of the stir zone, the <0001>//ND orientation (within 30-deg tolerance) was attributed to a shoulder-induced material flow, whereas the orientations with basal planes within 30-deg deviation from the tool probe were attributed to the probe-induced material flow. The remaining orientations were associated with the transitional material flow. Considering the above-discussed elliptical character of material motion at high temperatures, the transitional orientations in the welds produced at $T \geq 0.79\ T_m$ were also attributed to the tool probe. On the other hand, based on the textural analysis in Figures 6 and 7, the material flow in the bottom half of the stir zone was associated solely with the tool probe.

The measurement results are summarized in Figure 9. The material behavior was relatively complex. As expected, the material flow at the lowest welding temperatures was dominated by the tool probe. Nevertheless, a remarkable portion of the material motion could be explained in the terms of the "truncated cone" model, whereas the contribution of the tool shoulder was very low. With an increase in welding temperature, the fraction of the transitional and the shoulder components became enlarged at the expense of the probe fraction. Above ~ 0.75 T_m, however, the transitional material flow tended to disappear, thus increasing the portions of the probe and the shoulder. At temperatures exceeding ~ 0.8 T_m, only these two components contributed to the global material transportation, and their mutual fractions showed no noticeable changes.

IV. DISCUSSION

EBSD measurements clearly indicated that material flow in the entire studied temperature range was relatively complex consisting of the shoulder-induced and probe-induced components. At relatively low welding temperatures, it was additionally contributed by a transitional component originating from a synergetic effect of the shoulder and the probe. The effects of FSW temperature on these three components as well as local material flow near welding defects are briefly discussed below.

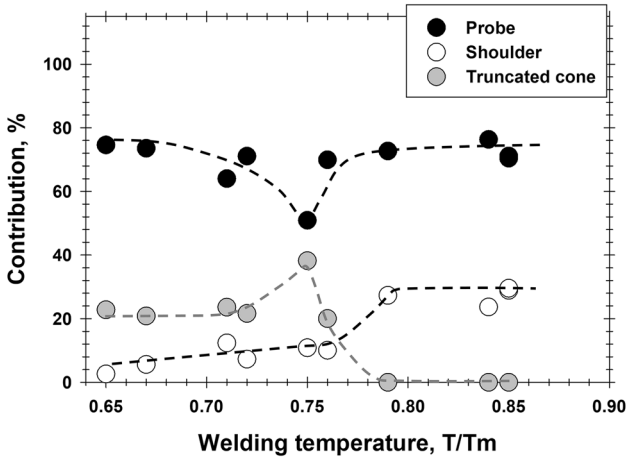

Fig. 9—Effect of welding temperature on contribution of different components of material flow. See Section III–B for details.

A. *Shoulder-Induced Material Flow*

The measured increase in the shoulder-induced component of material flow with welding temperature (Figure 9) may be directly linked with preferential enlargement of the sub-surface area of the stir zone (Figure 4(b)). The latter effect virtually indicated a preferential material softening occurring in this microstructural region during FSW. This observation was in the line with the widely accepted concept on the dominant role of the tool shoulder in generation of FSW heat suggested by Tang *et al.*[26]

On the other hand, the revealed phenomenon also suggests that generation of the heat in the upper section of the stir zone outpaced its subsequent propagation in material bulk. This may be due to the relatively low thermal conductivity of magnesium (160 W/m × K at ambient temperature *vs* 400 W/m × K in copper or 235 W/m × K in aluminum). In this context, an abrupt enhancement of the shoulder-induced material flow above ~0.8 T_m (Figure 9) may indicate a sharp reduction of thermal conductivity in this temperature range. It should be noted, however, that thermal characteristics of magnesium at such high temperatures are not studied well, to the best of the authors' knowledge, and therefore the above suggestion is totally speculative.

It should be also noted that the observed enhancement of the shoulder-induced material flow may also be associated with an increment of the tool plunge depth at high welding temperatures. This effect is normally observed during FSW operating under the *constant load condition* and may be ready attributed to material softening. Despite that the plunge depth in the current

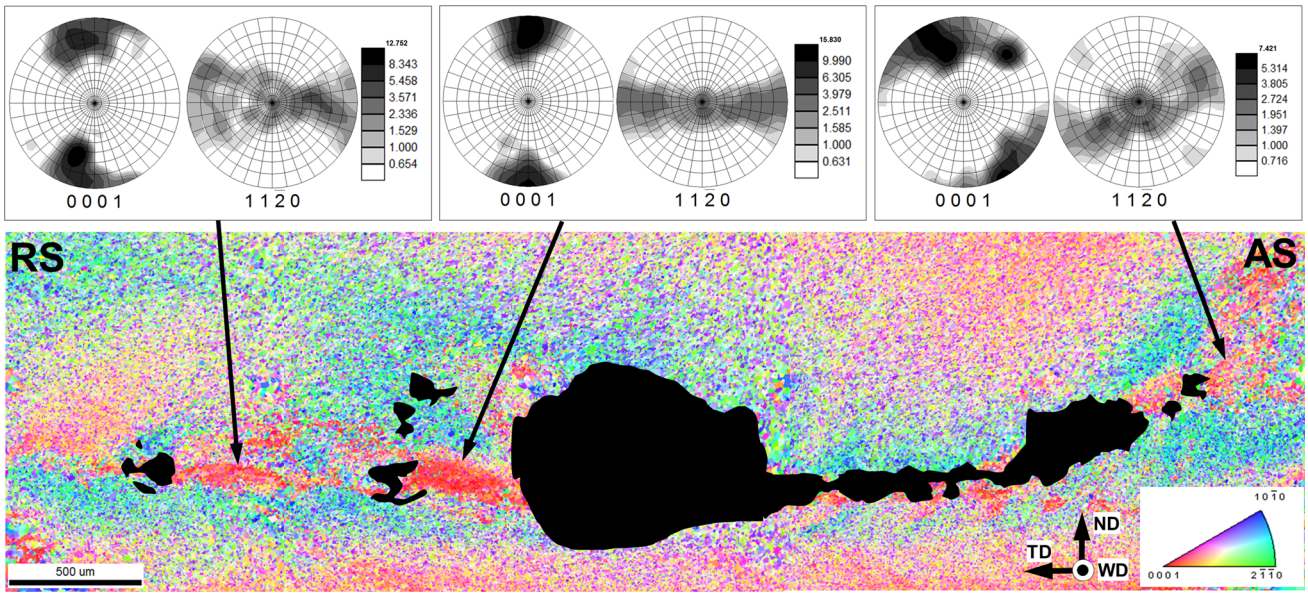

Fig. 10—High-resolution EBSD map along with (0001) and (11$\bar{2}$0) pole figures showing textural pattern near welding defects. The grains in the map are colored according to their crystallographic orientations relative ND; the color code triangle is shown in the bottom right corner. RS and AS are retreating side and advancing side, respectively. Note: the map was taken from the weld produced at the welding temperature of 0.75 T_m (weld pitch of 0.2 mm) (Color figure online).

study was set constant, the above effect perhaps cannot be completely excluded from consideration.

B. *Transitional Material Flow*

The relatively low thermal conductivity of magnesium should result in a temperature gradient throughout the stir zone thickness. To maintain the strain compatibility requirements between the shoulder- and probe-induced material movements, this should give rise to transitional material flow. In this context, the revealed vanishing of this component in high-temperature range (and the concomitant anomaly at ~ 0.75 T_m in Figure 7) was surprising.

This unexpected result may be explained by relatively low temperature sensitivity of flow stresses at very high deformation temperatures. In AZ31 magnesium alloy, this effect has been observed by Maksoud *et al.*[27] This should smooth the flow stress distribution within the stir zone and thus eliminate the transitional material flow. On the other hand, a reduction of the welding temperature should increase the temperature sensitivity of the flow stresses and thus even relatively small temperature gradient within the stir zone may give rise to the transitional material flow.

C. *Probe-Induced Material Flow*

One of the most significant effects of the welding temperature on probe-induced material flow was a transformation of the stir zone shape from cylindrical to elliptical one (Figure 3). This phenomenon was most likely a synergetic result of progressive material softening with welding temperature as well as the reduction of weld pitch (Table I) which should result in nearly rotational material motion at high welding temperatures. On the other hand, an alternative explanation for the elliptical-shaped stir zone in high-temperature welds may also be a forging action of the tool shoulder associated with a 3-deg tool tilting during FSW.

D. *Textural Patterns Near Welding Defects*

Attempting to get insight into the origin of the welding defects, high-resolution EBSD maps were taken from several defective regions and typical example is shown in Figure 10.

It is seen that the textural pattern near the defects was very complex and therefore the material flow in such areas was likely irregular. In all cases, however, distinct textural bands with orientation close to <0001>//ND were revealed. Considering the fact that the defects were typically found near the weld root (Figures 3(a) and (b)), this orientation was probably produced by the material extruded from under the probe tip. In other words, the welding defects may be associated with the so-called ring vortex material flow.[28] It is worth noting in this regard that such material motion is known to be essentially influenced by the tool geometry as well as its tilting angle (*e.g.,* Reference 29). Specifically, the tool tapering has been recently shown to lead to considerable variations in local strain rate[30] thus giving rise to concomitant stresses.

V. CONCLUSIONS

In this work, the influence of welding temperature on material flow during FSW of AZ31 magnesium alloy was studied. To this end, FSW trials were conducted in

the temperature interval of 0.65-0.85T_m and sample-scale EBSD mapping was employed to characterize texture distribution in the produced welds. Despite that the low-temperature welds were characterized by macro-scale defects (which presumably affected material flow and thus contaminated textural data), several important observations were made.

Due to specific design of the welding tool, material motion in the upper section of stir zone was essentially influenced by tool shoulder, whereas that in the remaining part of the weld was governed by the tool probe. In some cases, a synergetic effect of the shoulder and probe actions gave rise to a transitional material flow.

The effect of the tool shoulder on global material flow was found to significantly increase with welding temperature. This effect was explained in terms of dominant role of the shoulder in heat generation during FSW as well as to relatively low thermal conductivity of magnesium, both of which presumably leading to preferential material softening in the upper section of the welded sheets.

Above ~ 0.8 T_m, the transitional component of material flow was found to abruptly disappear. This phenomenon was suggested to originate from reduction of temperature sensitivity of flow stresses in high-temperature range and their concomitant equilibration throughout the weld thickness.

The welding defects were found to concentrate almost exclusively within the <0001>//ND textural bands. Accordingly, the defects were associated with the ring vortex material flow generated by the probe tip.

CONFLICT OF INTEREST

No potential conflict of interest was reported by the authors.

REFERENCES

1. R.S. Mishra and Z.Y. Ma: *Mater. Sci. Eng. R.*, 2005, vol. 50A, pp. 1–78.
2. R. Nandan, T. DebRoy, and H.K.D.H. Bhadeshia: *Prog. Mater. Sci.*, 2008, vol. 53, pp. 980–1023.
3. P.L. Threadgill, A.J. Leonard, H.R. Shercliff, and P.J. Withers: *Int. Mater. Rev.*, 2009, vol. 54, pp. 49–93.
4. U.F.H.R. Suhuddin, S. Mironov, Y.S. Sato, H. Kokawa, and C.-W. Lee: *Acta Mater.*, 2009, vol. 57, pp. 5406–18.
5. S. Mironov, Q. Yang, H. Takahashi, I. Takahashi, K. Okamoto, Y.S. Sato, and H. Kokawa: *Metall. Mater. Trans A.*, 2010, vol. 41A, pp. 1016–24.
6. R.W. Fonda and K.E. Knipling: *Sci. Tech. Weld. Join.*, 2011, vol. 16, pp. 288–94.
7. P.B. Prangnell and C.P. Heason: *Acta Mater.*, 2005, vol. 53, pp. 3179–92.
8. R.W. Fonda and J.F. Bingert: *Scr. Mater.*, 2007, vol. 57, pp. 1052–55.
9. Y.S. Sato, H. Kokawa, K. Ikeda, M. Enomoto, S. Jogan, and T. Hashimoto: *Metall. Mater. Trans. A*, 2001, vol. 32A, pp. 941–48.
10. D.P. Field, T.W. Nelson, Y. Hovanski, and K.V. Jata: *Metall. Mater. Trans. A*, 2001, vol. 32A, pp. 2869–77.
11. A.P. Reynolds, E. Hood, and W. Tang: *Scr. Mater.*, 2005, vol. 52, pp. 491–94.
12. T.U. Seidel and A.P. Reynolds: *Metall. Mater. Trans. A*, 2001, vol. 32A, pp. 2879–84.
13. K.N. Krishnan: *Mater. Sci. Eng. A*, 2002, vol. 327, pp. 246–51.
14. Y. Morisada, T. Imaizumi, and H. Fujii: *Sci. Technol. Weld. Join.*, 2015, vol. 20, pp. 130–37.
15. Y. Morisada, T. Imaizumi, and H. Fujii: *Scr. Mater.*, 2015, vol. 106 (2015), pp. 57–60.
16. T.U. Seidel and A.P. Reynolds: *Sci. Technol. Weld. Join.*, 2003, vol. 8, pp. 175–83.
17. R. Nandan, G.G. Roy, T.J. Lienert, and T. DebRoy: *Sci. Technol. Weld Join*, 2006, vol. 11, pp. 526–37.
18. H. Schmidt, T.L. Dickerson, and J. Hattel: *Acta Mater.*, 2006, vol. 54, pp. 1199–1209.
19. M. Guerra, C. Schmidt, J.C. McClure, L.E. Murr, and A.C. Nunes: *Mater. Character.*, 2002, vol. 49, pp. 95–101.
20. R. Crawford, G.E. Cook, A.M. Strauss, D.A. Hartman, and M.A. Stremler: *Sci. Technol. Weld. Join.*, 2006, vol. 11, pp. 657–65.
21. A.P. Reynolds: *Sci. Technol. Weld. Join.*, 2000, vol. 5, pp. 120–24.
22. S. Mironov, T. Onuma, Y.S. Sato, and H. Kokawa: *Acta Mater.*, 2015, vol. 100, pp. 301–12.
23. D.P. Field: *Ultramicroscopy*, 1997, vol. 67, pp. 1–9.
24. S.H.C. Park, Y.S. Sato, and H. Kokawa: *Metall. Mater. Trans. A.*, 2003, vol. 34A, pp. 987–94.
25. W. Tang, X. Guo, J.C. McClure, L.E. Murr, and A. Nunes: *J. Mater. Proc. Manuf. Sci.*, 1998, vol. 7, pp. 163–72.
26. I.A. Maksoud, H. Ahmed, and J. Rodel: *Mater. Sci. Eng. A.*, 2009, vol. 504, pp. 40–48.
27. J.A. Schneider and A.C. Nunes: *Metall Mater. Trans. B*, 2004, vol. 35B, pp. 777–83.
28. Y. Huang, Y. Wang, L. Wan, H. Liu, J. Shen, J.F. dos Santos, L. Zhou, and J. Feng: *Int. J. Adv. Manuf. Technol.*, 2016, vol. 87, pp. 1115–23.
29. M.M.Z. Ahmed, B.P. Wynne, W.M. Rainforth, A. Addison, J.P. Martin, and P.L. Threadgill: *Metall. Mater. Trans. A*, 2019, vol. 50A, pp. 271–84.
30. Y. Huang, Y. Xie, X. Meng, Z. Lv, and J. Cao: *J. Mater. Process. Technol.*, 2018, vol. 252, pp. 233–41.